AMERICAN SOCIETY FOR MICROBIOLOGY | Applied and Environmental Microbiology

Environmental Microbiology | Full-Length Text

Impact of mineral and non-mineral sources of iron and sulfur on the metalloproteome of *Methanosarcina barkeri*

James Larson,[1] Monika Tokmina-Lukaszewska,[1] Devon Payne,[2] Rachel L. Spietz,[2] Hunter Fausset,[1] Md Gahangir Alam,[2] Brooklyn K. Brekke,[1] Jordan Pauley,[1] Ethan J. Hasenoehrl,[1] Eric M. Shepard,[1] Eric S. Boyd,[2] Brian Bothner[1]

AUTHOR AFFILIATIONS See affiliation list on p. 17.

ABSTRACT Methanogens often inhabit sulfidic environments that favor the precipitation of transition metals such as iron (Fe) as metal sulfides, including mackinawite (FeS) and pyrite (FeS_2). These metal sulfides have historically been considered biologically unavailable. Nonetheless, methanogens are commonly cultivated with sulfide (HS^-) as a sulfur source, a condition that would be expected to favor metal precipitation and thus limit metal availability. Recent studies have shown that methanogens can access Fe and sulfur (S) from FeS and FeS_2 to sustain growth. As such, medium supplied with FeS_2 should lead to higher availability of transition metals when compared to medium supplied with HS^-. Here, we examined how transition metal availability under sulfidic (i.e., cells provided with HS^- as sole S source) versus non-sulfidic (cells provided with FeS_2 as sole S source) conditions impact the metalloproteome of *Methanosarcina barkeri* Fusaro. To achieve this, we employed size exclusion chromatography coupled with inductively coupled plasma mass spectrometry and shotgun proteomics. Significant changes were observed in the composition and abundance of iron, cobalt, nickel, zinc, and molybdenum proteins. Among the differences were alterations in the stoichiometry and abundance of multisubunit protein complexes involved in methanogenesis and electron transport chains. Our data suggest that *M. barkeri* utilizes the minimal iron-sulfur cluster complex and canonical cysteine biosynthesis proteins when grown on FeS_2 but uses the canonical Suf pathway in conjunction with the tRNA-Sep cysteine pathway for iron-sulfur cluster and cysteine biosynthesis under sulfidic growth conditions.

IMPORTANCE Proteins that catalyze biochemical reactions often require transition metals that can have a high affinity for sulfur, another required element for life. Thus, the availability of metals and sulfur are intertwined and can have large impacts on an organismismal biochemistry. Methanogens often occupy anoxic, sulfide-rich (euxinic) environments that favor the precipitation of transition metals as metal sulfides, thereby creating presumed metal limitation. Recently, several methanogens have been shown to acquire iron and sulfur from pyrite, an abundant iron-sulfide mineral that was traditionally considered to be unavailable to biology. The work presented here provides new insights into the distribution of metalloproteins, and metal uptake of *Methanosarcina barkeri* Fusaro grown under euxinic or pyritic growth conditions. Thorough characterizations of this methanogen under different metal and sulfur conditions increase our understanding of the influence of metal availability on methanogens, and presumably other anaerobes, that inhabit euxinic environments.

KEYWORDS iron acquisition, archaea, metallomics, metal regulation, proteomics, metalloproteins, methanogenesis, methanogens

Methanogens conserve energy through the metabolism of hydrogen (H_2), organic acids, or small methylated compounds, generating methane (CH_4) as a byproduct

Editor Isaac Cann, University of Illinois Urbana-Champaign, Urbana, Illinois, USA

Address correspondence to Brian Bothner, bbothner@montana.edu.

The authors declare no conflict of interest.

See the funding table on p. 18.

Received 21 March 2024
Accepted 27 June 2024
Published 18 July 2024

Copyright © 2024 American Society for Microbiology. All Rights Reserved.

Downloaded from https://journals.asm.org/journal/aem on 06 August 2024 by 153.90.170.23.

(1). Metabolism of these compounds is achieved through a conserved central methanogenesis pathway, with various add-on enzymes that enable the metabolism of diverse substrates (1). Methanogen metabolism is heavily reliant on metals, with methanogens requiring significantly more iron (Fe) per cell than other organisms based upon increased abundance of iron-sulfur ([Fe-S]) cluster motifs encoded in their genome (2). Beyond Fe, methanogens also require relatively large amounts of nickel (Ni), cobalt (Co), zinc (Zn), and molybdenum (Mo) compared to other prokaryotic organisms (3). Cobalt is a necessary metal cofactor in corrinoid methyltransferase proteins utilized in the methylotrophic pathway (4, 5). Previous work has shown that methanogenic activity in sludge bed reactors increased with the addition of Co when methanol was provided as substrate (6). Nickel is largely used in various [Ni-Fe] hydrogenases for the activation of H_2, and is additionally present in the tetrapyrrole cofactor F_{430} in methyl-coenzyme M reductase (MCR) (7, 8). Zinc is found in the ribosomal complexes of methanogens (3, 9), whereas Mo is used in enzymes to catalyze numerous redox reactions, including molybdenum nitrogenase and formylmethanofuran dehydrogenase (10–13). The prevalence of metals in methanogen metabolism motivates research to understand how metal bioavailability impacts their physiology and thus ecology.

Methanogens are common in environments that lack oxygen but are rich in sulfide (HS^-), also known as euxinic conditions (14). Euxinic conditions promote sulfidation of transition metals, ultimately resulting in the formation of sulfide minerals such as mackinawite (FeS) and pyrite (FeS_2) (15–18). Recently, representatives of both type 1 (i.e., *Methanococcus voltae* A3*, Methanococcus maripaludis* S2) and type 2 (*Methanosarcina barkeri* MS and Fusaro) methanogens have been shown to be capable of meeting their Fe and sulfur (S) requirements through the reductive dissolution of FeS_2 (14, 19, 20). However, the exact mechanism for Fe and S acquisition has not been fully elucidated. Comparative proteomics of type 1 (*M. voltae* A3) and type 2 (*M. barkeri* MS) methanogens grown on soluble Fe(II)/HS^- or FeS_2 as the sole Fe and S sources, respectively, show major changes in the proteomes of these organisms, in particular proteins involved in metal binding, metal uptake, and predicted Fe-trafficking and Fe-storage pathways (21, 22). Appendages attaching *M. voltae* cells to FeS_2 have been observed with field emission scanning electron microscopy when grown on FeS_2 mineral (20). Additional experiments with *M. barkeri* Fusaro demonstrated that the methanogen was unable to grow when cells were prevented physical access to FeS_2 (19). However, growth was supported when an exogenous electron shuttle (a synthetic quinone analog) was added to the growth medium (19). These data support a hypothesis wherein cells must either first attach to the mineral surface to facilitate extracellular electron transfer to facilitate mineral reduction or secrete electroactive shuttle compounds to facilitate mineral reduction (20).

Reduction of FeS_2 releases HS^- into solution and forms pyrrhotite ($Fe_{1-x}S$) on the mineral surface (19). Fe(II) (but not HS^-) then dissolves from $Fe_{1-x}S$ and reacts with the previously released HS^- to form aqueous FeS clusters (FeS_{aq}) that are predicted to be neutrally charged and thought to passively diffuse or be actively transported (if charged) across the membrane. After assimilation of FeS_{aq} into cells, Fe and S are trafficked and stored by largely uncharacterized mechanisms that may involve the formation of intracellular thioferrate-like minerals (14). Nonetheless, cells can synthesize protein-bound [Fe-S] clusters when grown on FeS_2 (14). Biosynthesis of [Fe-S] clusters in methanogens generally occurs via the sulfur (SUF) system in type I (non-cytochrome-encoding) methanogens or the SUF system and iron-sulfur cluster assembly (ISC) pathway in type II (cytochrome-encoding) methanogens (23, 24). It has previously been shown that all methanogens have the genetic capacity to generate [Fe-S] clusters through a minimal SUF system (SufCB). This system is comprised of an ATPase, SufC, and a scaffold protein, SufB (23). A recent phylogenetic analysis of over 10,000 archaeal and bacterial genomes revealed an additional minimalistic pathway called the minimal [Fe-S] cluster assembly (MIS) which requires fewer genes than the ISC system to synthesize and traffic [Fe-S] clusters with ISC-like proteins using a cysteine desulfurase, Mis-S, and a scaffold protein, Mis-U (25). Type II methanogens can encode both minimal [Fe-S]

Downloaded from https://journals.asm.org/journal/aem on 06 August 2024 by 153.90.170.23.

cluster synthesis pathways, posing new questions with respect to what types of growth conditions support the use of each of these [Fe-S] cluster biosynthetic pathways.

To begin to probe this question, and to better understand how growth with FeS_2 versus Fe(II)/HS^- influences the availability of transition metals and their use in the metalloproteome of methanogens, we employed size exclusion chromatography (SEC) in line with an inductively coupled plasma mass spectrometer (ICPMS) to detect changes in metalloproteins in cultures of *M. barkeri* Fusaro. In parallel, size exclusion chromatography was also used for fractionation of the proteome and the fractions were subsequently analyzed by tandem mass spectrometry for protein identification. This work shows that changes in the metalloproteome of *M. barkeri* cultured under the sulfidic conditions typically used to culture methanogens and those cultured with FeS_2 are surprisingly large for several transition metals, and include apparent major changes in the mechanism by which cells synthesize [Fe-S] clusters, synthesize cysteine, and generate a membrane potential.

MATERIALS AND METHODS

Culturing *Methanosarcina barkeri* Fusaro

Methanosarcina barkeri strain Fusaro (ATCC-BAA-2329) was grown in 75 mL of base salts medium as previously described (19). Acetate (40 mM) and methanol (0.5% vol/vol) were used as methanogenesis substrates under a headspace of N_2:CO_2 (80%:20%) pressurized to 2.5 bar. Growth medium was prepared without Fe and S in MilliQ water and using acid (10% HNO_3) washed glassware. Medium was amended with sulfide, added as Na_2S, to a final concentration of 1 mM and ferrous iron [Fe(II) added as $FeCl_2$] to a final concentration of 20 µM. Pyrite was synthesized as previously described (20). FeS_2 was added as a slurry to a final concentration of 2 mM Fe. Cultures were incubated in serum bottles statically on their sides and in the dark at 38°C. Cultures were inoculated from an exponentially growing culture. Once they reached early log phase, the cells were harvested under anoxic headspace by centrifugation at 4,600 × *g* for 30 min at 4°C. Then, the supernatant was decanted and cell pellet was flash frozen in liquid N_2. Frozen cell pellets were stored at −80°C until further analysis. Two control experiments were performed in the same fashion. The first control experiment was an abiotic experiment where growth medium and FeS_2 were incubated together. The second control experiment consisted of *M. barkeri* grown on FeS_2 (as above) but with exposure to 2 mM Na_2S for 15 min immediately prior to harvesting.

Methane (CH_4) in the headspace was quantified via an SRI 8610C gas chromatograph (SRI Instrument Company Inc., Torrance, CA) with the instrument injector valve set at 55°C using a Hayesep DB 100/120 packed column (Valco Instrument Company Inc., Houston, TX) with the oven set at 44°C. Helium (He) was used as the carrier gas and CH_4 was detected via a flame ionization detector set at 156°C. Standard curves to relate CH_4 peak area to concentration were made each day using certified standards (EGAS Depot, Nampa, ID). The concentration of HS^- (product of FeS_2 reduction) was determined colorimetrically on subsamples of culture via the methylene blue assay using a Genesys 10S Vis Spectrophotometer (ThermoScientific, Waltham, MA) (26).

M. barkeri grows in aggregates and this can confound direct enumeration of cells via microscopy (27). As such, growth of *M. barkeri* was monitored by quantification of genomic DNA as a proxy for cell production. To quantify DNA, 1 mL subsamples of *M. barkeri* Fusaro cultures were collected via sterile syringe and needle, transferred to sterile microfuge tubes, centrifuged at 20,000 × *g* for 20 min at 4°C, and then the supernatant was decanted. After centrifugation, the cell pellet was resuspended in a lysis buffer solution containing 489 µL sodium phosphate buffer (MP Biomedicals, Irvine, CA, USA) and 61 µL MT buffer (MP Biomedicals). The mixture was then gently stirred before three cycles of freezing at −80°C and heating/thawing at 52°C in a heat block. The mixture was then transferred to a 2 mL screw cap bead beating tube (MP Biomedicals) and homogenized for 40 s using a bead beater (Biospec Products, Bartlesville, OK, USA). To

Downloaded from https://journals.asm.org/journal/aem on 06 August 2024 by 153.90.170.23.

separate DNA from cell debris, bead beating tubes were centrifuged for 15 min at 14,000 × *g* at 4°C. The concentration of DNA was quantified using a Qubit HS Double-Stranded DNA kit and Qubit fluorimeter (Invitrogen, Carlsbad, CA, USA).

Protein extraction

Cell pellets were washed three times by gentle manual shaking in 5 mL of lysis solution (N_2 sparged 200 mM ammonium acetate; pH 8). Following each wash, cells were pelleted by centrifugation at 1,500 × *g* at 4°C for 5 min. Cell pellets were then resuspended in 800 µL of lysis buffer and lysed with matrix E (MPBio) on a FastPrep-24 5G bead beater (MPBio) using four 30-s cycles at a speed of 5.5 m/s with 1-min rest at room temperature (~21°C) in between cycles. Lysates were pelleted at 18,000 × *g* at 4°C for 20 min and supernatants were then filtered over 0.2 µm cellulose acetate filters using spin-X centrifuge tubes (Costar) at 24,700 × *g*. Protein concentrations were determined using the Bradford assay. Samples were analyzed immediately after cell lysis to minimize exposure to air.

Metalloproteome analysis

The metalloproteomes of *M. barkeri* Fusaro cells grown with FeS_2 or Fe(II)/HS^- were analyzed via SEC-ICPMS using an Agilent Infinity II LC coupled to an Agilent 7800 ICPMS, as previously described (28). Briefly, 95 µg of soluble protein was injected onto an Agilent Bio-SEC 3 (3 µm, 300 Å, 4.6 × 300 mm) column and proteins were separated for 25 min in N_2 sparged 200 mM ammonium acetate (pH 8) as the mobile phase with a flow rate of 0.4 mL/min. Ammonium acetate was used as the mobile phase because of its compatibility with SEC and ICPMS and its ability to not disrupt non-covalent interactions (29). The signals of ^{56}Fe, ^{59}Co, ^{60}Ni, ^{66}Zn, and ^{95}Mo were collected with an integration time of 1.5 s per element. Monitoring of ion signals was performed in Agilent MassHunter 4.7 (version C.01.06). The ICPMS parameters were as follows: RF power 1550 W, RF Matching 1.00 V, nebulizer Gas 0.99 L/min, option gas 0.0%, nebulizer pump 0.30 rps, S/C temp 2°C, makeup gas 0.00 L/min, extract 1 lens 0.0 V, extract 2 lens −195.0 V, omega bias −95 V, omega lens 8.4 V, cell entrance −40 V, cell exit −60 V, deflect 0 V, plate bias −55 V, He flow rate 4.0 mL/min, octupole bias −18 V, octupole RF 200 V, and energy discrimination 3.0 V. SEC-ICPMS data were normalized to the highest peak intensity for each metal.

ICPMS analysis of soluble cellular metals

To assess total cellular soluble metal content, 178 µg of protein was digested in 8% (wt/vol) optima grade HNO_3 (Fisher Chemical) for 20 min at 99°C. After digestion, samples were centrifuged at 16,000 × *g* at 4°C for 5 min and the supernatant was collected. Quantitative analysis was performed using an Agilent Infinity II autosampler coupled to an Agilent 7800 ICPMS in helium mode. One hundred microliters of supernatant was infused with the mobile phase (2% HNO_3, 0.5% HCl in water) with a flow rate of 1 mL/min. The signals of five metal ions were monitored for 30 s and included ^{56}Fe, ^{59}Co, ^{60}Ni, ^{66}Zn, and ^{95}Mo with an integration time/mass of 0.5 s per analyte.

Abiotic trace metal availability

An abiotic experiment was conducted to investigate the effect of different culture conditions on the availability of transition metals. The experiment was conducted in basal medium that lacked vitamins and methanol/acetate. Three different conditions were tested: soluble Fe(II) (20 µM) alone, soluble Fe(II) (20 µM) and sulfide (1 mM), or FeS_2 (2 mM). The trace element stock solution contained (g L^{-1}) $ZnCl_2$, 0.070; $MnCl_2 \cdot 4H_2O$, 0.100; H_3BO_3, 0.006; $CoCl_2 \cdot 6H_2O$, 0.190; $CuCl_2 \cdot 2H_2O$, 0.002; $NiCl_2 \cdot 6H_2O$, 0.024; $Na_2MoO_4 \cdot 2H_2O$, 0.036. All three experiments were amended with trace elements to a final concentration of 1 mL L^{-1}. After the amendments were added, the reactors were over-pressurized with 15 psi of 80:20 N_2:CO_2. The reactors were then sampled via syringe and needle (~1 hour after stock additions) and 3 mL of solution was filtered with a

Downloaded from https://journals.asm.org/journal/aem on 06 August 2024 by 153.90.170.23.

0.22 µm polytetrafluoroethylene (PTFE) membrane (ThermoFisher, Titan filters) into clean 15 mL tubes which were then frozen (t_0). The reactors were then incubated at 37°C for 4 days, after which the reactors were again sampled and the filtrates frozen (t_f). The filtrates were thawed and then acidified with trace-metal grade HNO_3 to 3% vol/vol. The samples were diluted directly prior to trace metal quantification via ICPMS to prevent salt-induced signal suppression.

SEC fractionation

SEC fractionation was carried out on an Agilent 1290 Infinity LC with an Agilent Infinity diode array detector using the same conditions as described for the SEC-ICPMS experiments. Biological replicates for each condition were concentration-matched, then equal volumes of replicates were pooled together. A total of 95 µg protein was injected onto an Agilent Bio-SEC 3 column (3 µm, 300 Å, 4.6 × 300 mm) and allowed to elute for 25 min at a flow rate of 0.4 mL/min. Beginning at 4 min post-injection, 1-min fractions were collected for 10 min. Collected fractions were freeze-dried for subsequent protein identification. Protein standards (cytochrome *c*, myoglobin, bovine serum albumin, γ-globulin, and glutamate dehydrogenase) were run in the same fashion as experimental samples. Their size exclusion elution, observed at 280 nm, was used as a molecular weight marker to generate estimated weight ranges for SEC fractions collected.

Proteomics of SEC fractions

The SEC fractions of the proteomes were freeze-dried prior to analysis by shotgun proteomics. The fractionated proteome samples (fractions 1–6) from both FeS_2 and Fe(II)/HS^- growth conditions were reduced, alkylated, and cleaned by chloroform/methanol extraction prior to digestion with sequencing grade modified porcine trypsin (Promega). Tryptic peptides were then separated by reverse phase XSelect CSH C18 2.5 µm resin (Waters) on an in-line 150 × 0.075 mm column using an UltiMate 3000 RSLCnano system (Thermo). Peptides were eluted using a 60-min gradient from 98:2 to 65:35 solution A:B ratio with solution A being 0.1% formic acid and 0.5% acetonitrile and solution B being 0.1% formic acid and 99.9% acetonitrile. Eluted peptides were ionized by electrospray (2.4 kV) followed by mass spectrometric analysis on an Orbitrap Eclipse Tribrid mass spectrometer (Thermo). MS data were acquired using the FTMS analyzer in profile mode at a resolution of 120,000 over a range of 375 to 1,400 m/z with advanced peak determination. Following HCD activation, MS/MS data were acquired using the ion trap analyzer in centroid mode and normal mass range with a normalized collision energy of 30%. Proteins were identified by database search using MaxQuant (Max Planck Institute) with a parent ion tolerance of 3 ppm and a fragment ion tolerance of 0.5 Da. Scaffold Q + S (Proteome Software) was used to verify MS/MS-based peptide and protein identifications. Protein identifications were accepted if they could be established with less than 1.0% false discovery and contained at least two identified peptides. Protein intensities were determined by the sum of the top 3 peptides of each protein. Protein probabilities were assigned by the Protein Prophet algorithm (30). Ratios of protein abundance in each SEC fraction were calculated between growth conditions based upon protein intensities (Table S1).

Identifications of metalloproteins

Identified proteins were submitted to the online functional annotation tool (DAVID) (31, 32) to generate functional annotations, gene ontology terms, ligand information, and protein domain classifications. The DAVID output file was searched for metal-related key words (i.e., iron, 4Fe-4S, zinc, molybdopterin, etc.) (Table S2). The intensities of predicted metal proteins from each fraction were then plotted to show protein abundance as a function of elution time (Tables S3 to S8).

Downloaded from https://journals.asm.org/journal/aem on 06 August 2024 by 153.90.170.23.

Gene synteny analysis of [Fe-S] cluster assembly system

Gene synteny was investigated using the *M. barkeri* Fusaro database in MetaCyc (33). A comparative gene synteny analysis was then conducted for other *Methanosarcina* species. For this, we used *Methanosarcina* sp. Kolksee and *Methanosarcina acetivorans* C2A gene databases on MetaCyc and additionally scanned the *Methanosarcina barkeri* MS genome (NCBI RefSeq assembly GCF_000970025.1) on the National Center for Biotechnology Information website (34).

RESULTS

Growth with different sources of Fe and S

Growth curves of *M. barkeri* Fusaro provided with Fe(II)/HS^- or FeS_2 as the sole Fe and S sources were generated to establish a baseline for growth under different mineral conditions. Analysis of the production of CH_4 and DNA (proxy for growth) shows that cells grew similarly between the two conditions, although growth was slightly better on Fe(II)/HS^- (Fig. S1a and b) as observed previously (19). This is likely due to the requirement that cells reduce FeS_2 prior to assimilation, which would require a diversion of electrons to the mineral surface (19). Total sulfide ($H_2S/HS^-/S^{2-}$) was calculated from the measured aqueous concentrations using Henry's law to account for headspace sulfide and found that the maximum amount of total sulfide released from the mineral was 1.04 to 1.31 µmol. Aqueous HS^- concentrations ranged from 0.73 µM to 9.71 µM with a maximum concentration observed at 4 days post-inoculation (Fig. S1c), consistent with reductive dissolution of FeS_2. Past experiments with FeS_2 under these incubation conditions have demonstrated no HS^- production in the absence of cells (19, 20). With these data in hand, the experiment was repeated to generate biomass for proteomic analysis with cells harvested at mid-log phase (i.e., 4 days).

Fe and S source alters the metalloproteome

The soluble protein fractions of *M. barkeri* Fusaro grown with Fe(II)/HS^- or FeS_2 were analyzed using SEC-ICPMS. The elution profiles of five metals critical for methanogens (^{56}Fe, ^{59}Co, ^{60}Ni, ^{66}Zn, and ^{95}Mo) were monitored by SEC-ICPMS and this revealed a wide distribution of metals putatively associated with proteins and protein complexes of low and high molecular weight in both conditions (Fig. 1; Fig. S2). Furthermore, this indicated that the protocol was capable of maintaining native protein and protein complex structures.

Next, the effect of different sources of Fe and S on putative Fe metalloproteins was investigated. There was an increased Fe signal in the FeS_2 condition throughout the entire elution profile (Fig. 1). The majority of the protein-bound Fe, in this condition, eluted early (4–5.5 min) (>300 kDa based on molecular weight standards). In contrast, Fe(II)/HS^- grown cells had a low-intensity Fe signal in this high molecular weight region with the majority of the protein-bound Fe eluting after 7 min. The large Fe peak was absent in abiotic control sample mimicking the FeS_2 growth condition (Fig. S3). SEC-ICPMS analysis of Fe(II)/HS^--grown cells exposed to FeS_2 before harvesting also lacked the large Fe signal observed in the FeS_2 growth condition. Together, the results show that the Fe present in the high molecular weight region of SEC elution profiles in cells grown on FeS_2 is a biological consequence of culturing these cells on the mineral substrate.

Next, protein-associated Co, Ni, and Zn were investigated (Fig. 1). In the FeS_2 condition, each of these metals had a low-intensity signal in the 4- to 6-min region which coincided with the large Fe peak. These metals had a large peak between 6 and 8 min. Cobalt and Ni also had broad maxima spanning the 8- to 11-min range that were absent in the Zn profile. In the Fe(II)/HS^--grown cells, the Co, Ni, and Zn profiles also looked very similar. Each signal increased in intensity around 6 min and plateaued until approximately 10 min for Co and Ni, and 8 min for Zn. The SEC-ICPMS metal profiles for FeS_2-grown cells and FeS_2-grown cells incubated with Fe(II)/HS^- were nearly identical (Fig. S4). The data demonstrate the metalloproteome from the FeS_2 condition has more Co, Ni,

Downloaded from https://journals.asm.org/journal/aem on 06 August 2024 by 153.90.170.23.

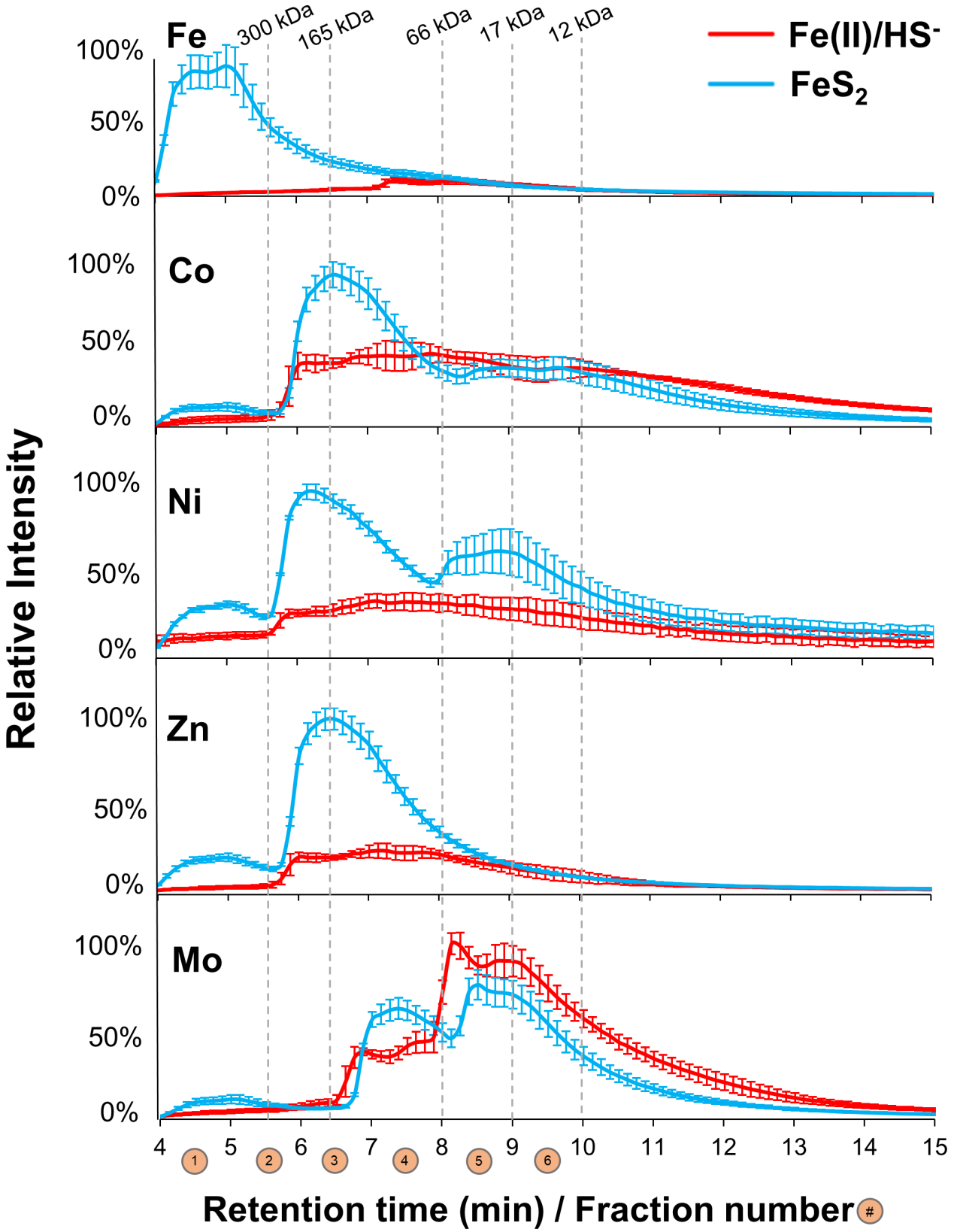

FIG 1 *Methanosarcina barkeri* metalloproteome response to Fe and sulfur (S) growth conditions. *M. barkeri* was grown on soluble ferrous iron (Fe(II)) and HS^- (red) or insoluble FeS_2 (blue). The soluble proteomes from both culture conditions were analyzed by SEC-ICPMS. The traces show the size distribution and intensity of protein-bound Fe, Co, Ni, Zn, and Mo. Error bars are ±1 standard deviation. SEC fractions are indicated by circles. Column void volume is at 4 min.

Downloaded from https://journals.asm.org/journal/aem on 06 August 2024 by 153.90.170.23.

and Zn than the Fe(II)/HS^- condition, and that this was not caused by residual HS^- during sample preparation.

The final metal analyzed was Mo (Fig. 1). The elution profiles for FeS_2 and Fe(II)/HS^- growth conditions were similar. Both growth conditions had a significant increase in Mo before 7 min, followed by multiple maxima through 11 min. A larger maxima was observed in the FeS_2 condition between 7 and 8 min, while the peaks after 8 min were higher in the Fe(II)/HS^- condition.

Fe and S source impacts metal uptake

The initial SEC-ICPMS analysis revealed differences in the metalloproteome between growth conditions. We used ICPMS to quantify total intracellular metal content (relative to protein concentration) to address whether these changes were the result of metal redistribution or a consequence of metal uptake. There was significantly more Fe, Ni, and Zn in the FeS_2 condition (*P*-value <0.05), but no significant difference in the Co abundance between conditions (Fig. S5). Interestingly, there was significantly more Mo in the Fe(II)/HS^- condition (*P*-value <0.05).

Sulfide alters metal solubility and availability

To assess differences in the availability of trace metals between growth conditions, abiotic reactors were set up with soluble Fe(II)/HS^- or with FeS_2 and analyzed with ICPMS (Fig. 2). Reactors containing Fe(II) without a S source served as a control. Comparison of the Fe(II)/HS^- samples with the control samples at the start of the experiment showed a significant decrease (P = 0.05) in Fe, Co, and Ni concentrations. Zn was undetected in the Fe(II)/HS^- samples, yet was detected in the control and FeS_2 samples. During this initial timepoint, only Fe and Co were significantly lower (P = 0.05) in the FeS_2 condition than the control condition. At this initial timepoint, Co and Ni were significantly higher (P = 0.05) in the FeS_2 condition than in the Fe(II)/HS^- condition. Zn was also detected in the FeS_2 condition. Meanwhile, both conditions saw additional changes after 4 days of incubation. Mo became significantly lower in the Fe(II)/HS^- condition than both the control and the FeS_2 condition. Ni concentrations were significantly higher in the Fe(II)/HS^- condition than in the FeS_2 condition, but both were much lower than the control. In both the Fe(II)/HS^- samples and the FeS_2 samples, Co was undetected in at least one of the replicates.

Identification of metalloproteins through shotgun proteomics

A total of 1,563 proteins [out of 3,698 open reading frames in the *M. barkeri* Fusaro genome (35)] were identified across all SEC fractions (Table S1). DAVID analysis returned information on the metal binding potential for 1,409 proteins (Table S2). One hundred forty-seven Fe proteins, 30 Ni proteins, 18 Mo proteins, 84 Zn proteins, and 25 Co proteins were identified in the SEC fractions collected (Tables S3 to S7). The results are broken out into target groups with predicted or characterized functions below.

Proteins putatively involved in Fe storage and trafficking in FeS_2-grown cells

To identify the protein responsible for the large molecular weight iron peak, we examined the fold-change (FeS_2:Fe(II)/HS^-) of the proteins identified in fraction 1. Only two of the identified proteins had changed over twofold: subunit K of A1AO H^+ ATPase Mbar_A0390 and the uncharacterized Mbar_A0933 (Table S1). BLAST analysis of Mbar_A0933 suggests it is a HEAT domain-containing protein. Neither protein contained canonical Fe-binding domains or motifs. The characterized Fe-binding proteins in fraction 1 did not have a significant change in abundance. We speculated that *M. barkeri* could store Fe as a thioferrate-like mineral in a large protein complex, similar to the IssA protein in *Pyrococcus furiosus* which lacks classical Fe-binding domains (36). *M. barkeri* Fusaro encodes two IssA homologs, Mbar_A1833 and Mbar_A1834. Both homologs were more abundant in the Fe(II)/HS^- condition (Fig. S6) and the elution time from SEC matched the expected protein size.

Downloaded from https://journals.asm.org/journal/aem on 06 August 2024 by 153.90.170.23.

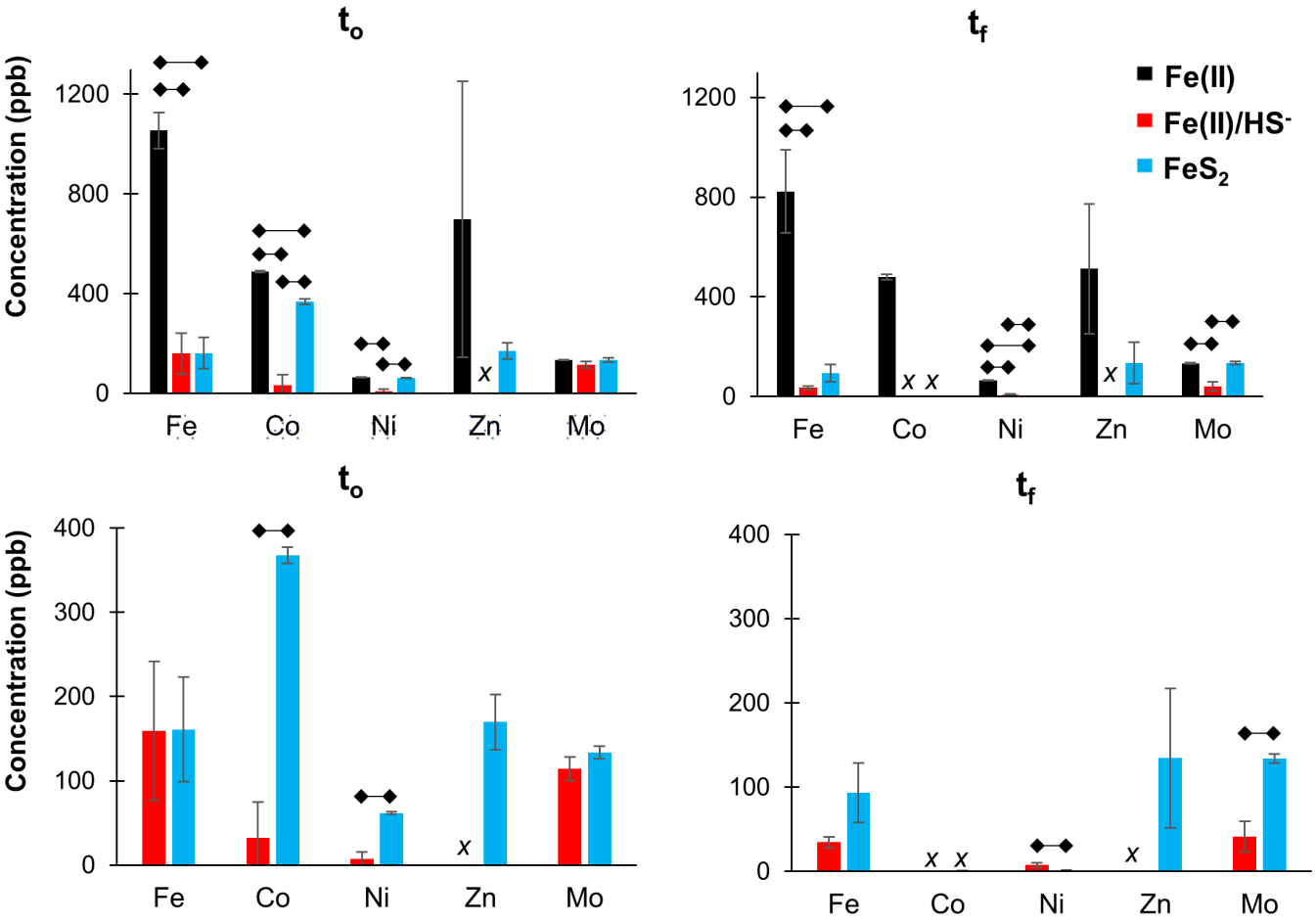

FIG 2 Influence of ferrous iron (Fe(II)), Fe(II) and HS^-, or FeS_2 on the availability of Fe, Co, Ni, Zn, and Mo. Metal concentrations from abiotic reactors were analyzed immediately after setting up the experiment (left, t_o) and after 4 days (right, t_f) for media containing trace metals and varying sources of iron and sulfur; soluble Fe(II) and no sulfur (black), soluble Fe(II)/HS^- (red), and mineral FeS_2 (blue). The bottom row is the same as the top row without displaying the soluble Fe(II) with no sulfur data for clarity. ◆—◆ indicates significant difference at *P*-value = 0.05. x indicates one or more samples were below the limit of detection.

Analysis of fractions 2–6 revealed the presence of two Fe-containing proteins that had an intensity ratio greater than fivefold (FeS_2:Fe(II)/HS^-) and shared a similar elution pattern across the sampled fractions (Fig. 3a). These proteins were initially identified as a cysteine desulfurase (Nif-S) homolog and an iron-sulfur cluster assembly protein (Nif-U) homolog. The genes for these two proteins reside next to each other on the *M. barkeri* Fusaro genome (Mbar_A2424 and Mbar_A2425). After examining the genomic context, it became evident that they could also be categorized in the recently described minimal [Fe-S] cluster assembly pathway as Mis-S and Mis-U, respectively (25). Bioinformatic analysis of the cysteine desulfurases of *M. barkeri* Fusaro, *M. acetivorans* C2A, and *Methanosarcina* sp. Kolksee revealed gene synteny with the MIS protein localization (Fig. 3b). The minimal [Fe-S] cluster mechanism SufCB was also identified in our data set. Both SufC (Mbar_A1078) and SufB (Mbar_A1079) were more abundant in the Fe(II)/HS^- condition (Fig. 4a). Interestingly, the elution patterns of these proteins were not uniform, as was observed for the MIS proteins.

Proteins involved in cysteine biosynthesis

The MIS genes that were upregulated in the FeS_2 condition are located between cysteine biosynthesis genes (Mbar_A2421, Mbar_A2422, and Mbar_A2427), a transcriptional regulator (Mbar_2423), and a hypothetical protein that was determined to be *nadA*

Downloaded from https://journals.asm.org/journal/aem on 06 August 2024 by 153.90.170.23.

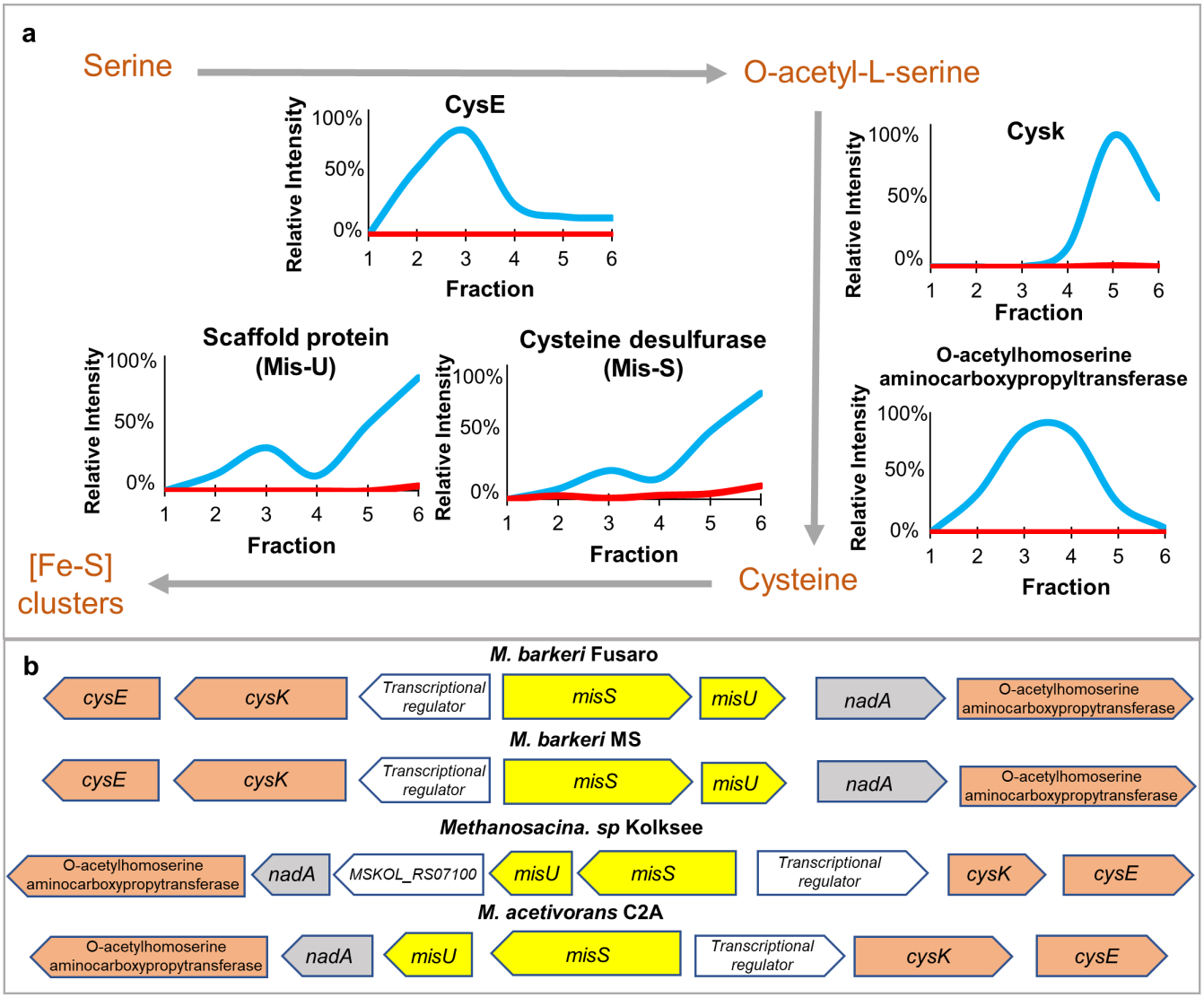

FIG 3 Fate of iron and sulfur in FeS_2-grown *Methanosarcina barkeri* cells. (a) Protein intensity of size exclusion chromatography fractions show an upregulation in cysteine biosynthesis and [Fe-S] cluster assembly pathway proteins in FeS_2-grown cells (blue) when compared to the Fe(II) and HS^- condition (red). Relative molecular weight ranges based upon standards; fraction 1 (460–970 kDa), fraction 2 (220–460 kDa), fraction 3 (100–220 kDa), fraction 4 (49–100 kDa), fraction 5 (23–49 kDa), and fraction 6 (11–23 kDa). (b) Analysis of the genomic context of cysteine desulfurase (MisS) and the scaffold protein (MisU) in *Methanosarcina barkeri* Fusaro, *Methanosarcina barkeri* MS, *Methanosarcina* sp. Kolksee, and *Methanosarcina acetivorans* C2A reveals gene synteny. Genes and genomes are adapted from Biocyc and NCBI databases and are not scaled to size. Conserved genes are color coordinated. The MIS system is in yellow, cysteine biosynthesis in salmon, and *nadA* in gray.

(Mbar_RS12880), which encodes for quinolate synthase A. The cysteine biosynthesis proteins were absent or in low abundance in the Fe(II)/HS^- fractions (Fig. 3a). These data show that under FeS_2 growth conditions, *M. barkeri* cysteine biosynthesis proteins and MIS proteins are more abundant. The localization of these genes in *M. barkeri* and the gene synteny across other *Methanosarcina* species suggests that these proteins work together in [Fe-S] cluster biosynthesis and respond to Fe availability. O-phospho-L-seryl-$tRNA^{Cys}$-tRNA synthase (Mbar_A1638), an enzyme involved in the alternative tRNA-dependent cysteine biosynthesis pathway, was present in our data and was more abundant in the Fe(II)/HS^- condition (Fig. 4b). While this enzyme was present in the FeS_2 growth condition, the elution profiles were different between conditions. In the Fe(II)/HS^- growth condition, it was bimodal with maxima in fractions 2 and 5, while in the FeS_2 condition, it was monomodal and centered between fractions 3 and 4. We observed

Downloaded from https://journals.asm.org/journal/aem on 06 August 2024 by 153.90.170.23.

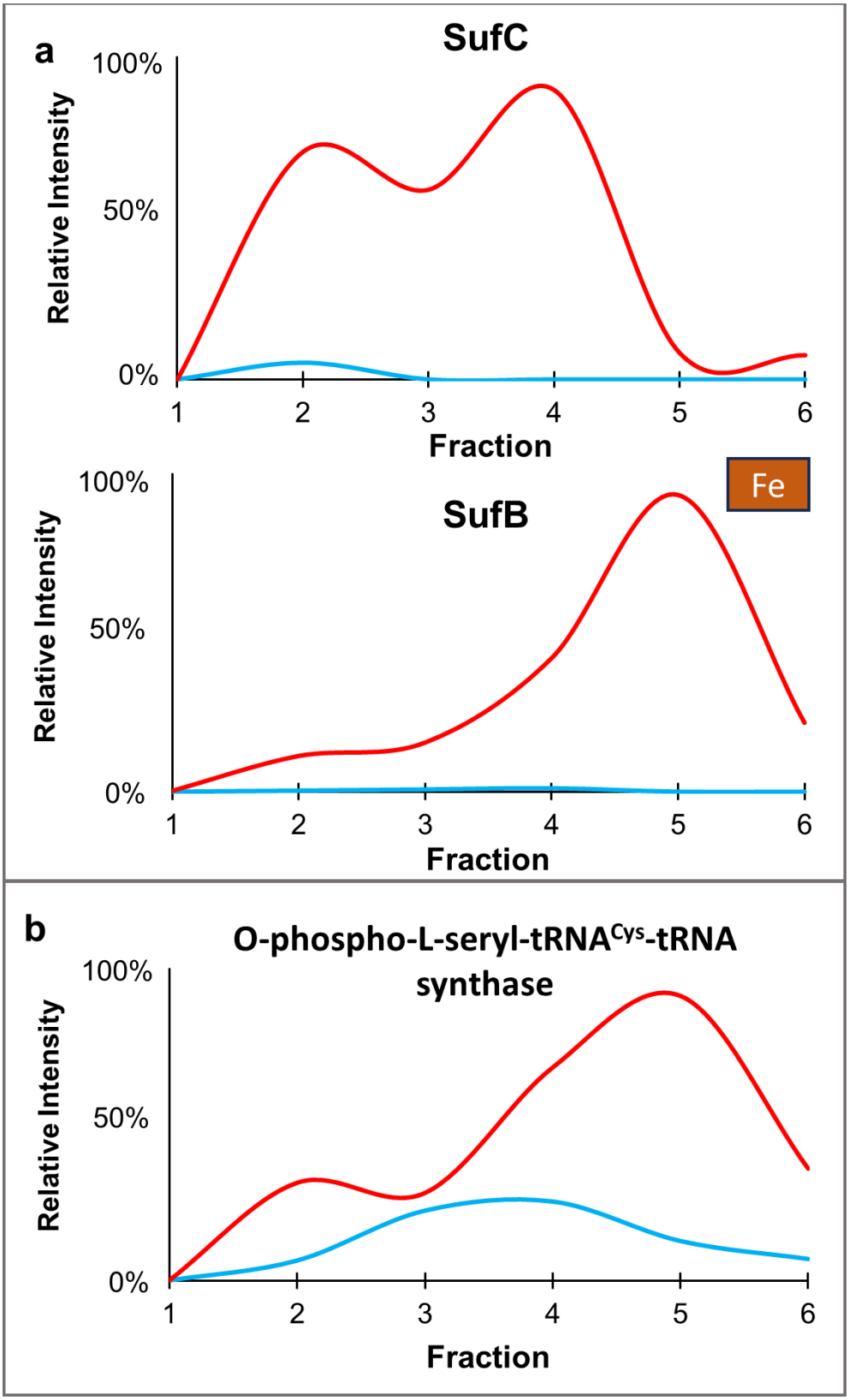

FIG 4 Influence of iron and sulfur source on iron-sulfur cluster assembly and cysteine biosynthesis protein intensity in *Methanosarcina barkeri* cells. Proteomics was done on individual size exclusion chromatography fractions for FeS_2 (blue)- or

(Continued on next page)

Downloaded from https://journals.asm.org/journal/aem on 06 August 2024 by 153.90.170.23.

FIG 4 (Continued)

Fe(II))/HS^- (red)-grown cells. Intensities of the identified proteins were plotted from each fraction for (a) Suf proteins and (b) O-phospho-L-seryl-tRNACys-tRNA synthase. Intensities were the average of the top 3 precursor ion intensities. Molecular weight ranges for each fraction: fraction 1 (460–970 kDa), fraction 2 (220–460 kDa), fraction 3 (100–220 kDa), fraction 4 (49–100 kDa), fraction 5 (23–49 kDa), and fraction 6 (11–23 kDa). Metal cofactors derived from DAVID functional annotation are given.

three other instances of cysteine desulfurases in the *M. barkeri* genome (Fig. S7). Two of these enzymes were not detected (Mbar_A3201, and Mbar_A1737) in the proteomics data (Fig. S7a). The other cysteine desulfurase (Mbar_A0729) was detected in equal abundance between conditions (Fig. S7b).

Proteins involved in methanogenesis and electron transport chains

The three subunits of MCR, alpha (Mbar_A0893, which contains nickel tetrapyrrole F_{430}), beta (Mbar_A0897), and gamma (Mbar_A0894), were detected in our proteomics data. All three subunits were more abundant in the FeS_2 growth condition and eluted with a unimodal SEC profile consistent with an assembled complex (Fig. 5a). The *mcr* locus encodes for two other Mcr proteins that are denoted McrC (Mbar_A0895) and McrD (Mbar_A0896). These two proteins had the opposite behavior in comparison to McrABG and were more abundant in the Fe(II)/HS^- condition. The bimodal elution profile indicates different oligomeric states (Fig. 5a). The change in Mcr inspired investigation of other core methanogenesis proteins. The subunits of coenzyme F_{420}-reducing [NiFe]-hydrogenase [alpha (Mbar_A0452), beta (Mbar_A0449), and gamma (Mbar_A0450)] were more abundant in the FeS_2 condition (Fig. 5b). Five corrinoid proteins (Mbar_A0945, Mbar_A3634, Mbar_A0842, Mbar_A740, Mbar_A1063), which are involved in the methylotrophic methanogenesis pathway, were identified in our data. Four of these corrinoid proteins were more abundant in the FeS_2 condition (Fig. 5c). These elution profiles show that the F_{420}-reducing [NiFe]- hydrogenase and most of the corrinoid proteins are higher in abundance in the FeS_2 condition.

A premise of this work was to maintain the native state of metalloprotein complexes. Therefore, our cell lysis and protein extraction methods were very gentle. This allowed us to retain several membrane protein complexes in the protein fraction. Among these were several membrane metalloproteins associated with methanogenesis and these were differentially expressed based on the growth condition. Methyltetrahydromethanopterin:coenzyme M methyltransferase (Mtr) is a membrane-bound complex that generates the ion motive force and the formation of methyl-CoM. Mtr is composed of eight subunits (MtrA-H) (37, 38). Six of these subunits were identified through the fractions: MtrA (Mbar_A1258 which binds Co), MtrB (Mbar_A1259), MtrC (Mbar_A1260), MtrE (Mbar_A1262), MtrG (Mbar_A1256), and MtrH (Mbar_A1255). The abundance of these subunits revealed that the stoichiometry of the complex was condition-dependent (Fig. 6a). In the Fe(II)/HS^- condition, there was a distinct bimodal distribution with maxima around fractions 2 and 4. In contrast, the distribution of these subunits in FeS_2 conditions was typically more broad with a larger single peak.

The elution profiles of energy-conserving [NiFe]-hydrogenase (Ech) show a change in both abundance and elution profile between culture conditions (Fig. 6b). In the Fe(II)/HS^- condition, there was a large Ech complex centered on fraction 2 and a smaller complex in fractions 4 and 5. EchB (Mbar_A0151) was the only subunit that had increased intensity in the smaller complex in the Fe(II)/HS^- condition. In the FeS_2 condition, all of the subunits, except EchA (Mbar_A0152) and EchC (Mbar_A0150), were more abundant in the smaller complex (fractions 4 and 5). In all cases, except for EchC and EchE (Mbar_A0148), protein abundance was higher in the Fe(II)/HS^- condition. The signal intensities for subunit EchC were very similar, while EchE was bimodal in the Fe(II)/HS^- condition with peaks in fractions 2 and 5 while being unimodal in the FeS_2 condition with a peak in fraction 4.

Downloaded from https://journals.asm.org/journal/aem on 06 August 2024 by 153.90.170.23.

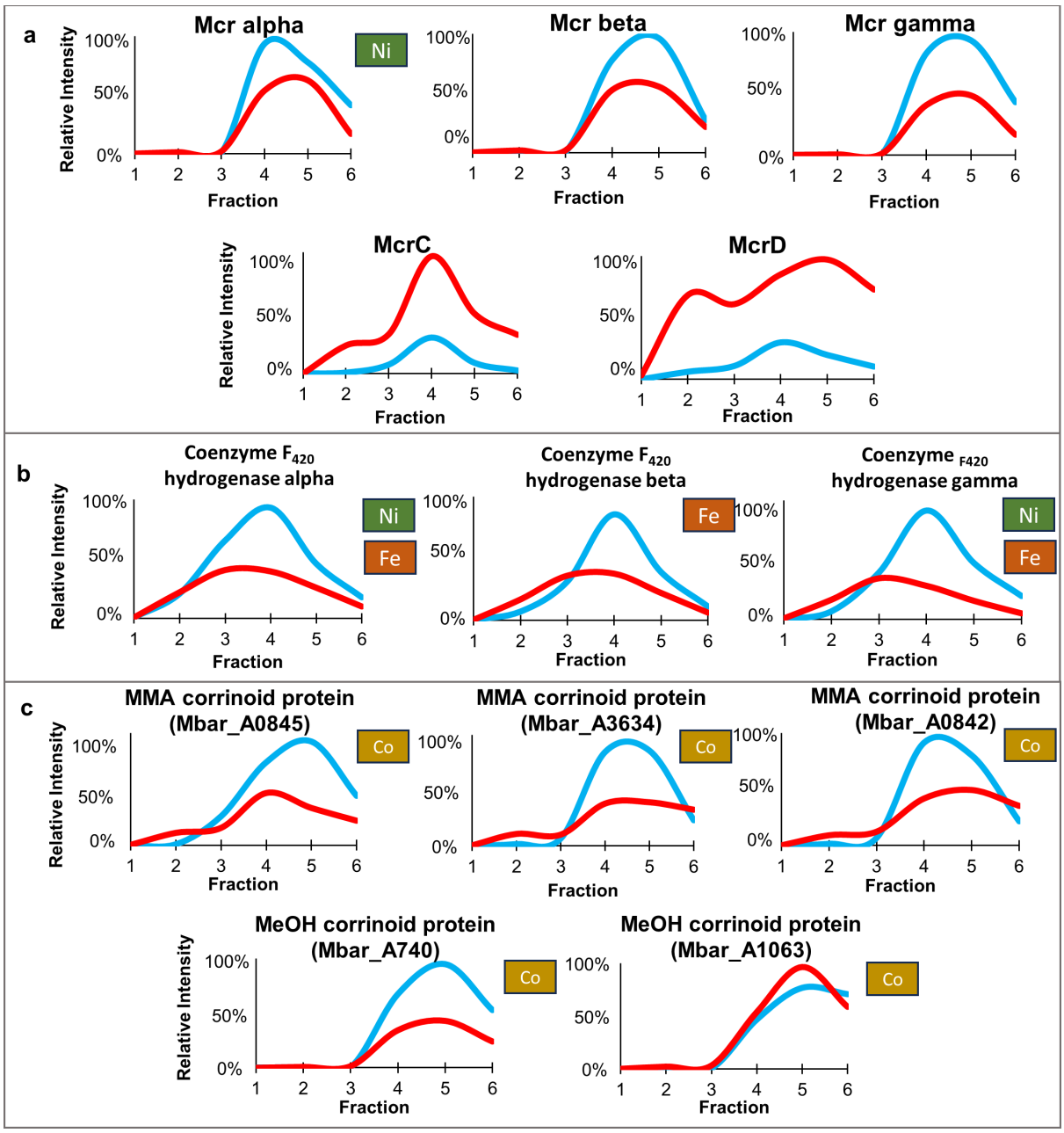

FIG 5 Source of iron and sulfur impacts methanogenesis protein intensities in SEC fractions. Proteomics was done on individual SEC fractions for FeS_2 (blue)- and Fe(II))/HS^- (red)-grown cells. Intensities of the identified soluble methanogenesis proteins were plotted from each fraction for (a) Mcr subunits, (b) F_{420}-reducing [NiFe]-hydrogenase subunits, and (c) corrinoid methyltransferase proteins. Locus tags are given for proteins. Monomethylamine is abbreviated as MMA and methanol is abbreviated as MeOH. Intensities were the average of the top 3 precursor ion intensities. Relative molecular weight ranges based upon standards: fraction 1 (460–970 kDa), fraction 2 (220–460 kDa), fraction 3 (100–220 kDa), fraction 4 (49–100 kDa), fraction 5 (23–49 kDa), and fraction 6 (11–23 kDa). Metal cofactors derived from DAVID functional annotation are given.

The elution patterns of the methanophenazine-reducing [NiFe]-hydrogenase (Vht) subunits were similar between conditions (Fig. 6c). There were increased intensities for the Vht large (Mbar_A1846) and small subunit (Mbar_A1847) in the Fe(II)/HS^- condition, but similar intensities for the cytochrome *b* subunit (Mbar_A1845). Heterodisulfide reductase (Hdr) subunits HdrD (Mbar_A1599) and HdrE (Mbar_A1598) were more abundant in the Fe(II)/HS^- condition (Fig. 6d). HdrD was bimodal in the Fe(II)/HS^- condition with peaks around fraction 2 and 4 but had a single peak in the FeS_2 condition

Downloaded from https://journals.asm.org/journal/aem on 06 August 2024 by 153.90.170.23.

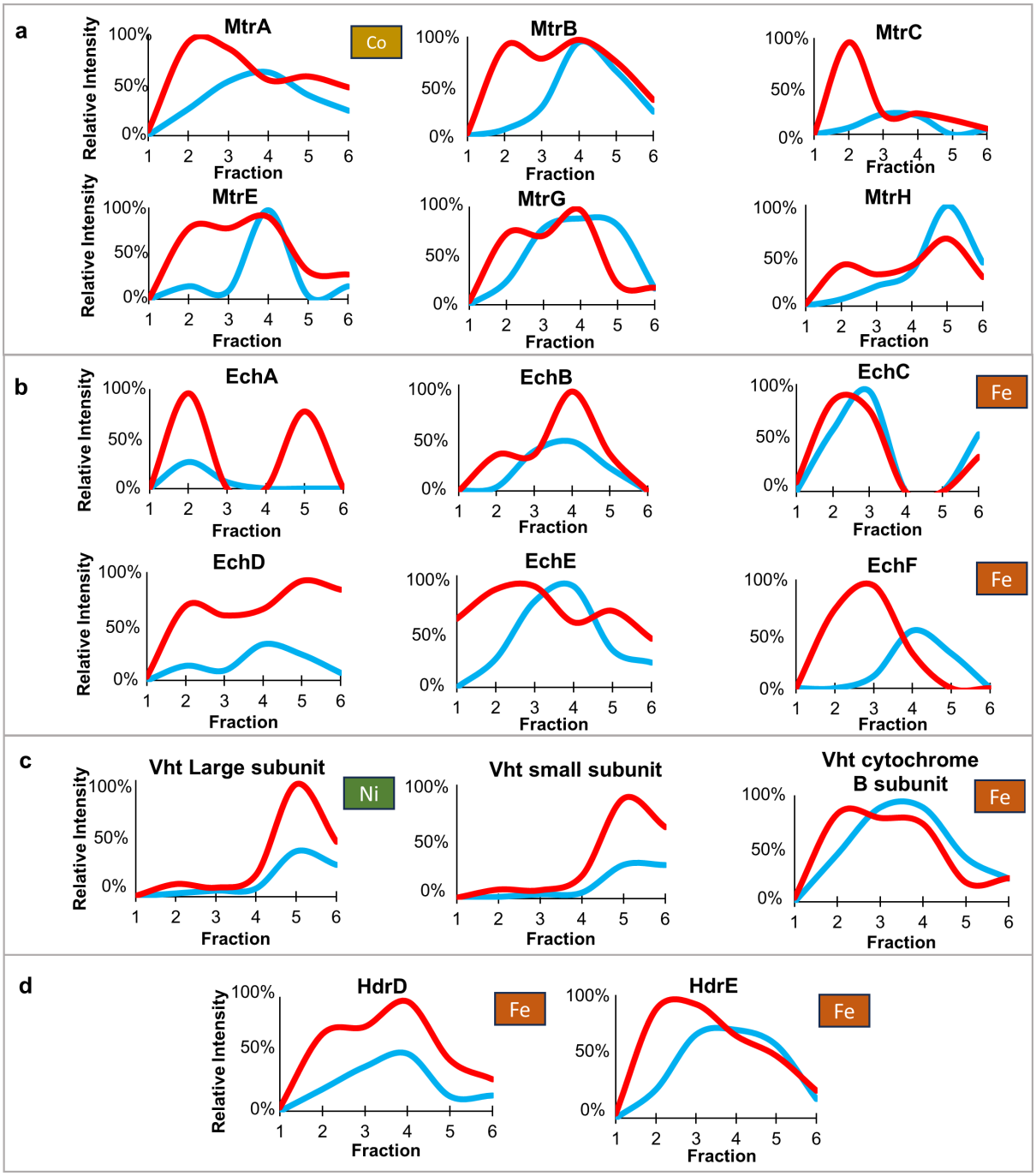

FIG 6 Iron and sulfur source alters membrane methanogenesis and electron transport chain proteins in SEC fractions. Proteomics was done on individual SEC fractions for FeS_2 (blue)- and Fe(II))/HS^- (red)-grown cells. Intensities of the identified membrane methanogenesis and electron transport proteins were plotted from each fraction for (a) Mtr subunits, (b) Ech subunits, (c) Vht subunits, and (d) Hdr subunits. Intensities were the average of the top 3 precursor ion intensities. Relative molecular weight ranges based upon standards: fraction 1 (460–970 kDa), fraction 2 (220–460 kDa), fraction 3 (100–220 kDa), fraction 4 (49–100 kDa), fraction 5 (23–49 kDa), and fraction 6 (11–23 kDa). Metal cofactors derived from DAVID functional annotation are given.

centered around fraction 4. In the FeS_2 condition, there was only one peak centered around fraction 4. HdrE had a large peak in fraction 2 in the Fe(II)/HS^- condition with peak tailing through the rest of the elution. In the FeS_2 condition, there was a broad peak centered around fraction 4. The elution profiles for these proteins show that the oligomeric state and abundance change for some of the proteins depending on the growth condition.

Downloaded from https://journals.asm.org/journal/aem on 06 August 2024 by 153.90.170.23.

Fe and S source affects ribosomal proteins

Five of the ribosomal proteins in the data set were annotated as Zn-containing proteins; three 50S proteins L24e (Mbar_A3386), L37Ae (Mbar_A2508), and L44e (Mbar_A1569), and two 30S proteins, S14 type Z (Mbar_A0096) and S27e (Mbar_A1568). These proteins have been shown to bind Zn in other organisms (39–42). The SEC distribution of these proteins differed between conditions (Fig. S8). L37Ae and S27e had a bimodal profile in the Fe(II)/HS^- condition but were unimodal in the FeS_2 condition. L44e, however, was unimodal in both conditions, but was present in earlier eluting fractions in the Fe(II)/HS^- condition, indicative of being part of a larger complex. L24e showed a similar distribution through the fractions between conditions, but was much higher in the Fe(II)/HS^- condition while being greatly reduced in the FeS_2 condition. S14 type Z showed a bimodal distribution in the Fe(II)/HS^- condition but is absent in the FeS_2 condition. There was also a change in distribution of ribonuclease J (Mbar_A1418), which also binds Zn. The elution profiles of these proteins show that the Fe and S source affects ribosomal proteins and protein complexes.

DISCUSSION

Methanogens commonly inhabit euxinic environments, conditions that favor the precipitation of many transition metals as sulfide minerals including Fe as FeS and FeS_2 (43). The recent discovery that *M. barkeri* and other methanogens can meet Fe and S demands directly from the minerals FeS and FeS_2 initiated a paradigm shift in how we think about metal availability in the environment and their acquisition in methanogens, and other organisms that inhabit euxinic environments (19, 20, 24). Our study aimed to characterize the difference in the metalloproteome of *M. barkeri* when grown with Fe(II)/HS^- (mimicking euxinic conditions) versus FeS_2. Importantly, in both conditions, Fe/S is in excess of cellular demands—potentially mitigating possible dosage effects due to the different availabilities of Fe and S. The concentrations used were based on past work (19, 20) that showed broad phenotypic changes in cells grown on Fe(II)/HS^- and FeS_2 so that detected changes in the metalloproteome could expand on these phenotypes. We leveraged an approach that profiled the metalloproteome while retaining the native structure of protein complexes using SEC coupled with ICPMS. SEC is a powerful tool for fractionating the proteome while maintaining complexes in the native state (Fig. S2) (44). Our data clearly show a restructuring of the metalloproteome in terms of metal distribution (Fig. 1), abundance of the metalloproteins involved in methanogenesis (Fig. 5), electron transport (Fig. 6), and ribosomal processes (Fig. S8) based on the source Fe and S provided. Furthermore, Fe(II)/HS^- and FeS_2 on their own were shown to alter the soluble metal pool (Fig. 2).

Metal availability and the structure of the metalloproteome are inherently linked (45, 46). Our data show that intracellular metal concentrations are dependent on the form of Fe and S that are available (Fig. S5). This appeared to be due in part to differential solubility of metals in the presence of Fe(II)/HS^- or FeS_2, independent of any biological mechanism. In abiotic reactors, soluble metal concentrations diminished in both conditions over a period of 4 days incubation. In the HS^- condition, this was due to the formation of metal sulfide precipitates, which were visually apparent and black in color, whereas in the FeS_2 condition, it was likely due to adsorption on the FeS_2 mineral (Fig. 2) (15–18). This finding implies that extra care must be taken when interpreting previous experimental regimes using Fe(II)/HS^- and metal accumulation in cells (47). The consequence of these different abiotic mechanisms, precipitation in the sulfide condition and adsorption in the FeS_2 condition, likely changes Co, Zn, Ni, and Mo acquisition strategies. This may facilitate acquisition of metals in the FeS_2 condition because they are colocalized with the FeS_2 surface, if not soluble (as was the case for Zn and Mo). This is supported by increased metal uptake of Fe, Ni, and Zn in the FeS_2-grown cells (Fig. S5) and increased intensities of these metals observed in the SEC-ICPMS data (Fig. 1). Cytosolic Co, however, was similar between conditions (Fig. S5), and abiotic reactors

Downloaded from https://journals.asm.org/journal/aem on 06 August 2024 by 153.90.170.23.

showed this element fully precipitated out of solution for both sources of Fe and S (Fig. 2). The observed changes in cytosolic metal concentrations and the metalloproteome are likely due to a dynamic multiplex response of metal acquisition and metabolic strategies. Indeed, large proteomic changes involving amino acid, protein, nucleic acid, and central carbon metabolism have been observed in *M. voltae* and *M. barkeri* MS in these same growth conditions leading to distinct phenotypes (21, 22).

Ribosomal protein expression was a major factor of phenotypic growth differences in *M. barkeri* MS grown under differing Fe and S sources (including FeS_2 and Fe(II)/HS^-) (21). It was speculated that this could be due to either differing growth rate kinetics between conditions or that these ribosomal proteins have moonlighting functions, performing non-ribosomal functions. In the FeS_2 growth experiments, *M. barkeri* Fusaro appears to use the recently proposed MIS cluster assembly to synthesize [Fe-S] clusters, as they were the only [Fe-S] cluster biosynthesis proteins in high abundance (Fig. 3a). The MIS consists of a cysteine desulfurase and a scaffold protein, but apparently no ATPase (25). The presence of these two proteins is significant because cysteine is the putative S source for the [Fe-S] clusters in this pathway (25). In contrast, the sulfidic growth experiments suggest that *M. barkeri* Fusaro uses the SufCB pathway for [Fe-S] cluster synthesis with the tRNA-dependent cysteine biosynthesis pathway (Fig. 4). The sulfur source for SufCB pathway has yet to be elucidated but could be FeS_{aq} clusters (either intact or dissolved), as has been recently proposed (14).

The different elution patterns between SufCB may be indicative of another protein involved in [Fe-S] cluster synthesis, potentially providing the unidentified sulfur source. Indeed, recent work investigating the role of these "minimal SUF" systems in a closely related strain, *Methanosarcina acetivorans,* has demonstrated they are not required for growth when HS^- or cysteine are provided as S sources potentially because these organisms also encode components of the ISC [Fe-S] biosynthetic system (48). Interestingly, the O-phospho-L-seryl-$tRNA^{Cys}$-tRNA synthase elution pattern has striking similarities to both SufC and SufB elution patterns (Fig. 4). This would provide a plausible explanation as to why *M. barkeri* uses the tRNA-dependent cysteine biosynthesis pathway with SufCB instead of the cysteine biosynthesis pathway used under FeS_2 growth conditions.

Based on previous results with *M. voltae* (14), we speculated that the large SEC-ICPMS Fe peak herein may be excess Fe that was being stored as thioferrate or a thioferrate-like mineral in supramolecular-IssA homolog structures to mitigate Fe toxicity (36). The two IssA homologs in *M. barkeri*, however, were low in abundance or not detected in the FeS_2 condition, yet were very abundant in the Fe(II)/HS^- condition (Fig. S6), suggesting they are not involved in coordination of this putative mineral in *M. barkeri*. This does not rule out the presence of thioferrate or a thioferrate-like mineral in the FeS_2 cells and may point to other functions of IssA homologs in *M. barkeri*. Alternatively, the IssA homologs could be post-translationally modified and therefore go undetected by the proteomics workflow used here. Another possibility is that one or both of the homologs may be tightly associated to the presumed thioferrate-like mineral, or binding in an orientation, that is not amenable to tryptic digestion.

The genetic differences between *M. voltae* and *M. barkeri* should not be ignored in the present interpretations. *M. voltae* is a type I methanogen and lacks homologs of cysteine desulfurase, while *M. barkeri* is a type II methanogen and has multiple homologs of cysteine desulfurase (49, 50). The ability of *M. barkeri* to metabolize cysteine to form [Fe-S] clusters may mitigate a need for Fe storage using IssA homologs. Our data, in the context of previous findings (14), suggest that Fe and S are trafficked differently in *M. barkeri* than in *M. voltae,* which may be due in part to the presence of a cysteine desulfurase and additional [Fe-S] biosynthetic machinery in the former organism.

A striking difference observed in our data was the expression of Mcr proteins. While there was higher abundance of the catalytic MCR subunits alpha, beta, and gamma in the FeS_2 condition, the McrC and McrD subunits were much higher in the Fe(II)/HS^- condition (Fig. 5a). There is little in the literature on the roles of McrC and McrD. McrC is

Downloaded from https://journals.asm.org/journal/aem on 06 August 2024 by 153.90.170.23.

necessary for activating MCR in *Methanothermobacter marburgensis* (51), and McrD has been proposed to be involved in MCR folding and cofactor insertion (52, 53). Since these proteins are working for the collective goal of supporting MCR folding and activation, we hypothesize that McrC and McrD are overexpressed in the Fe(II)/HS^- condition to compensate for the lower expression of MCR. Another possibility is that the species of Fe brought into cells when grown on FeS_2 versus those grown with HS^- differs and leads to different needs for these McrC and McrD proteins in MCR complex formation.

The findings of our research highlight the complex interplay between metal availability in the environment, cellular acquisition, metabolism, and metalloproteome composition. *M. barkeri* employs different metabolic strategies when grown under Fe(II)/HS^- and FeS_2 growth conditions. These metabolic strategies have significant effects on the metalloproteome and protein complexes involved in numerous essential functions including methanogenesis and [Fe-S] cluster biosynthesis. Our work also shows a connection between the MIS and cysteine biosynthesis pathway when *M. barkeri* is grown under FeS_2 conditions which are distinct from the SufCB and t-RNA-dependent cysteine biosynthesis pathways employed when grown under euxinic conditions. The consequence of this may influence Fe trafficking and storage. This work provides important and new insights into the mechanisms used by methanogens to acquire essential Fe and S and highlights exciting new areas for future investigation into metal and S acquisition under different environmental conditions. Additionally, the plasticity of the metalloproteome observed here should motivate additional study into the redistribution of the metalloproteome and stoichiometry of protein complexes of other microorganisms that occupy a multitude of diverse environment types where essential transition metals are expected to be differentially available.

ACKNOWLEDGMENTS

This work was supported by the Division of Chemical Sciences, Geosciences, and Biosciences, Office of Basic Energy Sciences of the US Department of Energy through Grant DE-SC0020246 to E.S.B., E.M.S., and B.B.

We would like to acknowledge the IDeA National Resource for Quantitative Proteomics lab at University of Arkansas for Medical Science for their help with the shotgun proteomics data analysis which was made possible through their National Institute of General Medical Sciences grant (R24GM137786). We would also like to thank Don Smith, Jesse Thomas, and Laura Dobeck of the Montana State University Core Facility for their help with ICPMS and SEC-ICPMS analyses.

Funding for the Montana State Mass Spectrometry Facility used in this publication was made possible in part by the MJ Murdock Charitable Trust, the National Institute of General Medical Sciences of the National Institutes of Health under award numbers P20GM103474 and S10OD28650, and the MSU Office of Research and Economic Development.

The content is solely the responsibility of the authors and does not necessarily represent the official views of the National Institutes of Health.

AUTHOR AFFILIATIONS

[1]Department of Chemistry and Biochemistry, Montana State University, Bozeman, Montana, USA
[2]Department of Microbiology and Cell Biology, Montana State University, Bozeman, Montana, USA

AUTHOR ORCIDs

James Larson http://orcid.org/0000-0001-9920-7682
Rachel L. Spietz https://orcid.org/0000-0001-5277-0734
Eric S. Boyd http://orcid.org/0000-0003-4436-5856
Brian Bothner http://orcid.org/0000-0003-1295-9609

Downloaded from https://journals.asm.org/journal/aem on 06 August 2024 by 153.90.170.23.

FUNDING

Funder	Grant(s)	Author(s)
U.S. Department of Energy (DOE)	DE-SC0020246	Eric M. Shepard Eric S. Boyd Brian Bothner
HHS | National Institutes of Health (NIH)	P20GM103474,S10OD28650	Brian Bothner

DATA AVAILABILITY

The identified proteins and their UniProt accession numbers and alternate identifiers are available in the supplemental tables. *M. barkeri* gene names for proteins of interest are given throughout the text.

ADDITIONAL FILES

The following material is available online.

Supplemental Material

Supplemental figures (AEM00516-24-s0001.pdf). Figures S1 to S8.
Supplemental tables (AEM00516-24-s0002.xlsx). Tables S1 to S8.

REFERENCES

1. Costa KC, Leigh JA. 2014. Metabolic versatility in methanogens. Curr Opin Biotechnol 29:70–75. https://doi.org/10.1016/j.copbio.2014.02.012
2. Major TA, Burd H, Whitman WB. 2004. Abundance of 4Fe–4S motifs in the genomes of methanogens and other prokaryotes. FEMS Microbiol Lett 239:117–123. https://doi.org/10.1016/j.femsle.2004.08.027
3. Glass JB, Orphan VJ. 2012. Trace metal requirements for microbial enzymes involved in the production and consumption of methane and nitrous oxide. Front Microbiol 3:61. https://doi.org/10.3389/fmicb.2012.00061
4. Ferry JG. 1999. Enzymology of one-carbon metabolism in methanogenic pathways. FEMS Microbiol Rev 23:13–38. https://doi.org/10.1111/j.1574-6976.1999.tb00390.x
5. Burke SA, Krzycki JA. 1997. Reconstitution of monomethylamine:coenzyme M methyl transfer with a corrinoid protein and two methyltransferases purified from *Methanosarcina barkeri*. J Biol Chem 272:16570–16577. https://doi.org/10.1074/jbc.272.26.16570
6. Zandvoort MH, Geerts R, Lettinga G, Lens PNL. 2002. Effect of long-term cobalt deprivation on methanol degradation in a methanogenic granular sludge bioreactor. Biotechnol Prog 18:1233–1239. https://doi.org/10.1021/bp020078e
7. Craft JL, Horng YC, Ragsdale SW, Brunold TC. 2004. Nickel oxidation states of F430 cofactor in methyl-coenzyme M reductase. J Am Chem Soc 126:4068–4069. https://doi.org/10.1021/ja038082p
8. Thauer RK, Kaster AK, Goenrich M, Schick M, Hiromoto T, Shima S. 2010. *Hydrogenases from Methanogenic Archaea, Nickel, a Novel Cofactor, and H2 Storage*. Available from: https://doi.org/101146/annurev.biochem030508152103
9. Sauer K, Thauer RK. 2000. Methyl-coenzyme M formation in methanogenic archaea. Eur J Biochem 267:2498–2504. https://doi.org/10.1046/j.1432-1327.2000.01245.x
10. Peng T, Xu Y, Zhang Y. 2018. Comparative genomics of molybdenum utilization in prokaryotes and eukaryotes. BMC Genomics 19:691. https://doi.org/10.1186/s12864-018-5068-0
11. Karrasch M, Börner G, Thauer RK. 1990. The molybdenum cofactor of formylmethanofuran dehydrogenase from *Methanosarcina barkeri* is a molybdopterin guanine dinucleotide. FEBS Lett 274:48–52. https://doi.org/10.1016/0014-5793(90)81326-j
12. Grahame DA, Stadtman TC. 1987. Carbon monoxide dehydrogenase from *Methanosarcina barkeri*. disaggregation, purification, and physicochemical properties of the enzyme. J Biol Chem 262:3706–3712.
13. Leigh JA. 2000. Nitrogen fixation in methanogens: the archaeal perspective. Curr Issues Mol Biol 2:125–131.
14. Payne D, Shepard EM, Spietz RL, Steward K, Brumfield S, Young M, Bothner B, Broderick WE, Broderick JB, Boyd ES. 2021. Examining pathways of iron and sulfur acquisition, trafficking, deployment, and storage in mineral-grown methanogen cells. J Bacteriol 203:e0014621. https://doi.org/10.1128/JB.00146-21
15. Bhattacharyya D, Jumawan AB, Grieves RB. 1979. Separation of toxic heavy metals by sulfide precipitation. Sep Sci Techn 14:441–452. https://doi.org/10.1080/01496397908058096
16. Lewis AE. 2010. Review of metal sulphide precipitation. Hydrometallurgy 104:222–234. https://doi.org/10.1016/j.hydromet.2010.06.010
17. Peltier E, Ilipilla P, Fowle D. 2011. Structure and reactivity of zinc sulfide precipitates formed in the presence of sulfate-reducing bacteria. Appl Geochem 26:1673–1680. https://doi.org/10.1016/j.apgeochem.2011.04.024
18. Estay H, Barros L, Troncoso E. 2021. Metal sulfide precipitation: recent breakthroughs and future outlooks. Minerals 11:1385. https://doi.org/10.3390/min11121385
19. Spietz RL, Payne D, Kulkarni G, Metcalf WW, Roden EE, Boyd ES. 2022. Investigating abiotic and biotic mechanisms of pyrite reduction. Front Microbiol 13:878387. https://doi.org/10.3389/fmicb.2022.878387
20. Payne D, Spietz RL, Boyd ES. 2021. Reductive dissolution of pyrite by methanogenic archaea. ISME J 15:3498–3507. https://doi.org/10.1038/s41396-021-01028-3
21. Fausset H, Spietz RL, Cox S, Cooper G, Spurzem S, Tokmina-Lukaszewska M, DuBois J, Broderick JB, Shepard EM, Boyd ES, Bothner B. 2024. A shift between mineral and nonmineral sources of iron and sulfur causes proteome-wide changes in *Methanosarcina barkeri*. Microbiol Spectr 12:e0041823. https://doi.org/10.1128/spectrum.00418-23
22. Steward KF, Payne D, Kincannon W, Johnson C, Lensing M, Fausset H, Németh B, Shepard EM, Broderick WE, Broderick JB, Dubois J, Bothner B. 2022. Proteomic analysis of *Methanococcus voltae* grown in the presence of mineral and nonmineral sources of Iron and sulfur. Microbiol Spectr 10. https://doi.org/10.1128/spectrum.01893-22
23. Boyd ES, Thomas KM, Dai Y, Boyd JM, Outten FW. 2014. Interplay between oxygen and Fe–S cluster biogenesis: insights from the suf pathway. Biochemistry 53:5834–5847. https://doi.org/10.1021/bi500488r
24. Johnson C, England A, Munro-Ehrlich M, Colman DR, DuBois JL, Boyd ES. 2021. Pathways of iron and sulfur acquisition, cofactor assembly,

Downloaded from https://journals.asm.org/journal/aem on 06 August 2024 by 153.90.170.23.

destination, and storage in diverse archaeal methanogens and alkanotrophs. J Bacteriol 203:e0011721. https://doi.org/10.1128/JB.00117-21
25. Garcia PS, D'Angelo F, Ollagnier de Choudens S, Dussouchaud M, Bouveret E, Gribaldo S, Barras F. 2022. An early origin of iron–sulfur cluster biosynthesis machineries before earth oxygenation. Nat Ecol Evol 6:1564–1572. https://doi.org/10.1038/s41559-022-01857-1
26. Fogo JK, Popowsky M. 1949. Spectrophotometric determination of hydrogen sulfide. Anal. Chem 21:732–734. https://doi.org/10.1021/ac60030a028
27. Sowers KR, Boone JE, Gunsalus RP. 1993. Disaggregation of *Methanosarcina* spp. and growth as single cells at elevated osmolarity. Appl Environ Microbiol 59:3832–3839. https://doi.org/10.1128/aem.59.11.3832-3839.1993
28. Larson J, Tokmina-Lukaszewska M, Fausset H, Spurzem S, Cox S, Cooper G, Copié V, Bothner B. 2023. Arsenic exposure causes global changes in the metalloproteome of *Escherichia coli*. Microorganisms 11:382. https://doi.org/10.3390/microorganisms11020382
29. Patterson A, Zhao Z, Waymire E, Zlotnick A, Bothner B. 2020. Dynamics of hepatitis B virus capsid protein dimer regulate assembly through an allosteric network. ACS Chem Biol 15:2273–2280. https://doi.org/10.1021/acschembio.0c00481
30. Nesvizhskii AI, Keller A, Kolker E, Aebersold R. 2003. A statistical model for identifying proteins by tandem mass spectrometry. Anal Chem 75:4646–4658. https://doi.org/10.1021/ac0341261
31. Sherman BT, Hao M, Qiu J, Jiao X, Baseler MW, Lane HC, Imamichi T, Chang W. 2022. DAVID: a web server for functional enrichment analysis and functional annotation of gene lists. Nucleic Acids Res 50:W216–W221. https://doi.org/10.1093/nar/gkac194
32. Huang DW, Sherman BT, Lempicki RA. 2009. Systematic and integrative analysis of large gene lists using DAVID bioinformatics resources. Nat Protoc 4:44–57. https://doi.org/10.1038/nprot.2008.211
33. Caspi R, Billington R, Keseler IM, Kothari A, Krummenacker M, Midford PE, Ong WK, Paley S, Subhraveti P, Karp PD. 2020. The metacyc database of metabolic pathways and enzymes - a 2019 update. Nucleic Acids Res 48:D445–D453. https://doi.org/10.1093/nar/gkz862
34. NCBI. *Methanosarcina barkeri* MS genome assembly ASM97002v1 - NCBI - NLM. Available from: https://www.ncbi.nlm.nih.gov/datasets/genome/GCF_000970025.1. Retrieved 3 Mar 2024. Accessed March 3, 2024
35. Maeder DL, Anderson I, Brettin TS, Bruce DC, Gilna P, Han CS, Lapidus A, Metcalf WW, Saunders E, Tapia R, Sowers KR. 2006. The *Methanosarcina barkeri* genome: comparative analysis with *Methanosarcina acetivorans* and *Methanosarcina mazei* reveals extensive rearrangement within methanosarcinal genomes. J Bacteriol 188:7922–7931. https://doi.org/10.1128/JB.00810-06
36. Vaccaro BJ, Clarkson SM, Holden JF, Lee D-W, Wu C-H, Poole Ii FL, Cotelesage JJH, Hackett MJ, Mohebbi S, Sun J, Li H, Johnson MK, George GN, Adams MWW. 2017. Biological iron-sulfur storage in a thioferrate-protein nanoparticle. Nat Commun 8:16110. https://doi.org/10.1038/ncomms16110
37. Kurth JM, Op den Camp HJM, Welte CU. 2020. Several ways one goal—methanogenesis from unconventional substrates. Appl Microbiol Biotechnol 104:6839–6854. https://doi.org/10.1007/s00253-020-10724-7
38. Welte C, Deppenmeier U. 2014. Bioenergetics and anaerobic respiratory chains of aceticlastic methanogens. Biochimica et Biophysica Acta (BBA) - Bioenergetics 1837:1130–1147. https://doi.org/10.1016/j.bbabio.2013.12.002
39. Nanamiya H, Kawamura F. 2010. Towards an elucidation of the roles of the ribosome during different growth phases in *Bacillus subtilis*. Biosci Biotechn Biochem 74:451–461. https://doi.org/10.1271/bbb.90859
40. Herve du Penhoat C, Atreya HS, Shen Y, Liu G, Acton TB, Xiao R, Li Z, Murray D, Montelione GT, Szyperski T. 2004. The NMR solution structure of the 30S ribosomal protein S27e encoded in gene RS27_ARCFU of *Archaeoglobus fulgidis* reveals a novel protein fold. Protein Sci 13:1407–1416. https://doi.org/10.1110/ps.03589204
41. Krishna SS, Majumdar I, Grishin NV. 2003. SURVEY AND SUMMARY: structural classification of zinc fingers. Nucleic Acids Res 31:532–550. https://doi.org/10.1093/nar/gkg161
42. Grishin NV. 2001. Treble clef finger—a functionally diverse zinc-binding structural motif. Nucleic Acids Res 29:1703–1714. https://doi.org/10.1093/nar/29.8.1703
43. Liu Y, Beer LL, Whitman WB. 2012. Methanogens: a window into ancient sulfur metabolism. Trends Microbiol 20:251–258. https://doi.org/10.1016/j.tim.2012.02.002
44. Kirkwood KJ, Ahmad Y, Larance M, Lamond AI. 2013. Characterization of native protein complexes and protein isoform variation using size-fractionation-based quantitative proteomics. Mol Cell Proteomics 12:3851–3873. https://doi.org/10.1074/mcp.M113.032367
45. Hay Mele B, Monticelli M, Leone S, Bastoni D, Barosa B, Cascone M, Migliaccio F, Montemagno F, Ricciardelli A, Tonietti L, Rotundi A, Cordone A, Giovannelli D. 2023. Oxidoreductases and metal cofactors in the functioning of the earth. Essays Biochem 67:653–670. https://doi.org/10.1042/EBC20230012
46. Dupont CL, Butcher A, Valas RE, Bourne PE, Caetano-Anollés G. 2010. History of biological metal utilization inferred through phylogenomic analysis of protein structures. Proc Natl Acad Sci U S A 107:10567–10572. https://doi.org/10.1073/pnas.0912491107
47. Scherer P, Lippert H, Wolff G. 1983. Composition of the major elements and trace elements of 10 methanogenic bacteria determined by Inductively coupled plasma emission spectrometry. Biol Trace Elem Res 5:149–163. https://doi.org/10.1007/BF02916619
48. Saini J, Deere TM, Lessner DJ. 2023. The minimal SUF system is not required for Fe–S cluster biogenesis in the methanogenic archaeon *Methanosarcina acetivorans*. Sci Rep 13:15120. https://doi.org/10.1038/s41598-023-42400-x
49. Lyu Z, Lu Y. 2018. Metabolic shift at the class level sheds light on adaptation of methanogens to oxidative environments. ISME J 12:411–423. https://doi.org/10.1038/ismej.2017.173
50. Liu Y, Sieprawska-Lupa M, Whitman WB, White RH. 2010. Cysteine is not the sulfur source for iron-sulfur cluster and methionine biosynthesis in the methanogenic archaeon *Methanococcus maripaludis*. J Biol Chem 285:31923–31929. https://doi.org/10.1074/jbc.M110.152447
51. Prakash D, Wu Y, Suh SJ, Duin EC. 2014. Elucidating the process of activation of methyl-coenzyme M reductase. J Bacteriol 196:2491–2498. https://doi.org/10.1128/JB.01658-14
52. Chadwick GL, Joiner AMN, Ramesh S, Mitchell DA, Nayak DD. 2023. McrD binds asymmetrically to methyl-coenzyme M reductase improving active-site accessibility during assembly. Proc Natl Acad Sci U S A 120. https://doi.org/10.1073/pnas.2302815120
53. Lyu Z, Chou CW, Shi H, Wang L, Ghebreab R, Phillips D, Yan Y, Duin EC, Whitman WB. 2018. Assembly of methyl coenzyme M reductase in the methanogenic archaeon *Methanococcus maripaludis*. J Bacteriol 200:e00746-17. https://doi.org/10.1128/JB.00746-17

Downloaded from https://journals.asm.org/journal/aem on 06 August 2024 by 153.90.170.23.